

Metal-insulator transition at the LaAlO₃/SrTiO₃ interface revisited: A hybrid functional study

F. Cossu and U. Schwingenschlögl*

KAUST, PSE Division, Thuwal 23955-6900, Kingdom of Saudi Arabia

V. Eyert†

Experimental Physics VI, Center for Electronic Correlations and Magnetism,
Institute of Physics, University of Augsburg, 86135 Augsburg, Germany

(Dated: November 5, 2018)

We investigate the electronic properties of the LaAlO₃/SrTiO₃ interface using density functional theory. In contrast to previous studies, which relied on (semi-)local functionals and the GGA+*U* method, we here use a recently developed hybrid functional to determine the electronic structure. This approach offers the distinct advantage of accessing both the metallic and insulating multilayers on a parameter-free equal footing. As compared to calculations based on semilocal GGA functionals, our hybrid functional calculations lead to a considerably increased band gap for the insulating systems. The details of the electronic structure show substantial deviations from those obtained by GGA calculations. This casts severe doubts on all previous results based on semilocal functionals. In particular, corrections using rigid band shifts (“scissors operator”) cannot lead to valid results.

I. INTRODUCTION

One of the most studied heterostructures in recent years is the oxide multilayer structure, which is formed from the two bulk insulators LaAlO₃ (LAO) and SrTiO₃ (STO). Unlike its bulk constituents, the ground state of the interface has been found to be conducting¹ and magnetic². In particular, already early studies reported the formation of an electron gas confined to a layer of only a few nanometers at the electron doped *n*-type interface³. The pronounced two-dimensional character of this layer has recently been confirmed⁴. In general, the nature and spatial confinement of two-dimensional electron gases has been the subject of extensive research^{5–12}. Interest in the LAO/STO interface stems from the exciting potential for applications due to the high mobility of the charge carriers, which makes the material a promising building block for field-effect devices^{13,14}. Following an early suggestion of Breitschaft and coworkers¹⁵ the electron system at the *n*-type interface is now widely regarded as an electron liquid due to strong electronic interactions.

A striking characteristic of the LAO/STO interface is the existence of a critical thickness of the LAO overlayer, below which the system is insulating. However, the exact number of LAO overlayers necessary to drive this thickness-dependent insulator-metal transition is still controversially discussed¹⁶. Early measurements of the sheet carrier density indicate that conduction sets in at an LAO thickness of four unit cells¹⁷. Applying hard x-ray photoelectron spectroscopy to samples grown under the same conditions as those of Thiel *et al.*, Sing *et al.* find the onset of a finite sheet carrier density already at a thickness of two LAO layers¹⁸. In addition, they find a further increase of the sheet carrier density on increasing the overlayer thickness. In contrast, Thiel *et al.* report that the sheet carrier density remains essentially constant once the critical thickness of four layers

has been reached. First principles local density approximation (LDA) calculations by Chen *et al.* confirm the onset of a finite conductivity at four LAO layers. Yet, these authors estimate that the critical thickness would be rather at five layers or beyond if band gap corrections were included¹⁶.

A strong influence of the oxygen content on the sheet carrier density has been established by Brinkman *et al.*² as well as Kalabukhov *et al.*¹⁹. Pavlenko *et al.* investigated especially the magnetic ordering at the interface^{20,21}. Yet, as has been pointed out by Basletic *et al.*, the electron gas arising from oxygen vacancies is of a pronounced three-dimensional character²².

Recent studies¹⁰ have confirmed that the formation of the two-dimensional electron liquid proceeds in three steps: (1) an orbital reconstruction due to broken inversion symmetry and the polarity of the interface, (2) polarization triggering a crystal reconstruction by means of Ti ion displacement, and (3) creation of a two-dimensional electron liquid due to charge from the overlayer. In this context, many theoretical studies on the influence of the overlayer thickness on the distortions have been performed^{23–26}. The dependence of the structural distortions on the type of interface has also been investigated by *ab initio* studies²⁷. The existence of the two-dimensional electron gas has been theoretically confirmed^{9,25,26} and was attributed to metal-induced gap states²⁸.

As a matter of fact, *ab initio* calculations with conventional local or semilocal exchange-correlation functionals underestimate the optical band gap of semiconductors and insulators. Yet, hybrid functionals have recently overcome this problem in large part and are known to accurately reproduce the experimental band gap of bulk LAO and STO. Hence, they can also be expected to better describe the band gap dependence in the LAO/STO heterostructure as a function of the overlayer thickness. However, this methodology is computationally very de-

manding and, hence, has been rarely applied to large structures as the present LAO/STO heterostructure. An exception is the recent work by Delugas and coworkers⁹. Yet, these authors concentrated on periodic LAO/STO heterostructures, where the LAO and STO layers are both sandwiched by the respective other material and thus the LAO layer is not a true surface layer.

In the present work we close the gap and employ hybrid functional calculations to correctly access the electronic properties of an LAO/STO heterostructure with the LAO layer terminated by a vacuum region. In doing so, we consider different thicknesses of the LAO overlayer in order to determine the critical number of layers, at which the insulator-metal transition sets in. While thus going beyond most previous studies, our results question the validity of calculations based on (semi-)local functionals.

II. COMPUTATIONAL DETAILS

The calculations were performed using the Vienna *Ab initio* Simulation Package (VASP)²⁹. The exchange-correlation functional was considered at the level of the generalized gradient approximation (GGA)³⁰. In addition, calculations as based on the recently developed hybrid functionals were performed in order to access the electronic properties. Within the framework of the generalized Kohn-Sham scheme³¹ these functionals combine the exchange functional as arising from the LDA with the non local Hartree-Fock expression. In the present work, the functional proposed by Heyd, Scuseria, and Ernzerhof (HSE) was used³². In this approach, the short-range part of the exchange functional is represented by a (fixed) combination of GGA- and Hartree-Fock contributions, while the long-range part and the correlation functional are described by the GGA only. The single-particle equations were solved using the projector-augmented wave method^{33,34} with a plane-wave basis with a cutoff of 400 eV. The force tolerance was set to 0.05 eV/Å and the energy tolerance for the self-consistency loop to 10^{-5} eV. The Brillouin zone was sampled at a grid of $4 \times 4 \times 1$ \mathbf{k} -points.

The structural setup consists of a central region of SrTiO₃, which comprises $5\frac{1}{2}$ unit cells and is terminated by TiO₂ layers. This region is sandwiched by two to six unit cells of LaAlO₃ on each side with AlO₂ layers at the surfaces and, hence, LaO layers at the n -type interfaces. We will refer to these systems in the following as IF 2 to IF 6. The sandwiches are separated by ≈ 20 -Å thick vacuum layers. As a consequence, the whole slab has inversion symmetry and is free of artificial dipoles. The in-plane lattice parameter was adopted from an initial full structural optimization of bulk SrTiO₃ at the GGA level, which resulted in a value of 3.944 Å and was kept in all calculations. In contrast, the atomic positions were all fully relaxed.

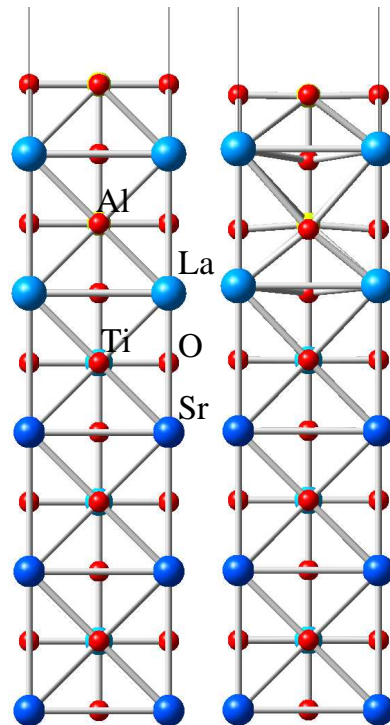


FIG. 1. Initial idealized (left) and optimized (right) structures with $5\frac{1}{2}$ central layers of SrTiO₃ sandwiched between two layers of LaAlO₃ from each side.

IF 2	IF 3	IF 4	IF 5	IF 6
+0.025	+0.030	+0.032	+0.036	+0.036
-0.331	-0.344	-0.337	-0.288	-0.265
-0.141	-0.116	-0.110	-0.089	-0.074
-0.193	-0.262	-0.270	-0.230	-0.205
	-0.159	-0.133	-0.107	-0.091
	-0.187	-0.252	-0.223	-0.196
		-0.159	-0.114	-0.092
		-0.183	-0.214	-0.196
			-0.135	-0.094
			-0.146	-0.188
				-0.119
				-0.131

TABLE I. Bucklings (in Å) of the atomic layers in the LaAlO₃ region of the systems IF 2 to IF 6, starting from the surface. Positive/negative signs denote a shift of the cations with respect to the anions off/to the surface.

III. RESULTS

Starting from ideal structures, which are derived from the geometry of bulk SrTiO₃ and, hence, consist of perfectly flat atomic layers with an equal spacing of 1.972 Å, we first note an overall vertical shrinking of the structures during the structural optimization. In addition, we observe distortions of the oxygen octahedra in all three

parts of the sandwiches. While the displacements of the basal O are towards the interface in both the STO and LAO regions, the displacements of the apical O are always towards the center of the sandwich, i.e. away from the interface and towards the interface in the STO and LAO regions, respectively. Whereas there is almost no buckling of the layers in the central STO region, the buckling is strong in the LAO regions with alternating short and long bond lengths between the cations and the apical O atoms. In general, the alternation of the bond lengths results in an elongation and flattening of all octahedra towards and away from the interface, respectively. The buckling in the LAO regions is stronger for the LaO layers than for the AlO_2 layers, with both Al and La atoms being farther away from the interface as compared to the basal O atoms of the respective layers. For the interface with two LAO layers the initial and optimized structures are sketched in Fig. 1. In addition, Table I summarizes the bucklings encountered in the different systems under investigation.

On moving away from the interface, the buckling of the LaO and AlO_2 increases and decreases, respectively. The AlO_2 surface layer also has an inward relaxation, which is stronger than that of the other layers (the inward relaxation, accumulated over all layers, determines the shrinking of the slab). Differences arise for the largest system under study, which contains six layers of LaAlO_3 on either side of the sandwich. Here, the TiO_2 layers have a weak but non-negligible buckling and the surface AlO_2 layer has a buckling, which is opposite to that of the other AlO_2 layers. The asymmetry of the octahedra is less pronounced for the LAO regions and in the STO region it is opposite to that of the other Ti-centered octahedra.

Since a full structural relaxation is not feasible using hybrid functionals due to the huge computational cost, we continue using the optimized structure obtained from the GGA calculations. However, the hybrid functional calculations still allow one to calculate the forces on the atoms. Finite forces obtained from the HSE functional would then indicate additional forces due to the improved treatment of the exchange interaction. According to our calculations this interaction leads to additional forces acting on the Ti and Al atoms, which point towards the interface. In other words, these atoms would move towards the center of the octahedra. This finding is in line with the results of previous GGA $+U$ calculations²³.

According to the total DOS as calculated with the hybrid functional and shown in Fig. 2, the insulator-metal transition occurs between four and five unit cells of LAO. In contrast, the GGA calculation give a metallic state already at four unit cells. This is in agreement with existing experimental data whereas the optical band gap of 0.6 eV arising from the HSE calculations clearly signals insulating behavior. Surprisingly, the situation is not unlike that of Ge, where calculations using local or semilocal functionals lead to metallic behavior, while hybrid functional calculations perfectly reproduce the experimental band gap of 0.66 eV. We thus argue that given our calcu-

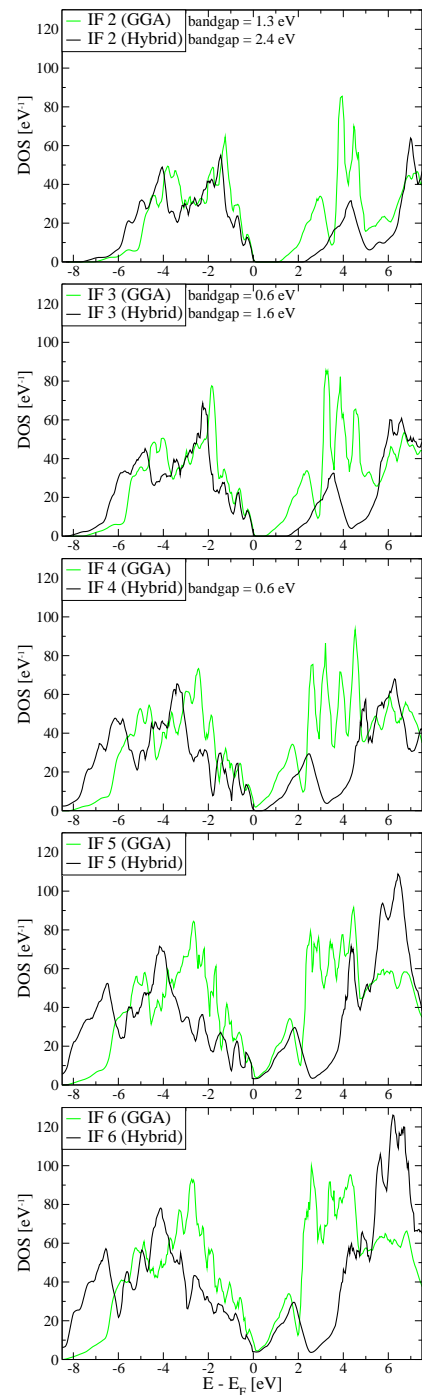


FIG. 2. Total DOSs for LAO thicknesses of two to six unit cells obtained in the GGA and hybrid functional calculations. The exact gap values are given, for the insulating systems.

lated results it is worthwhile rechecking the experimental data with respect to the exact number of layers at the transition.

Despite the difference in absolute value the optical band gaps arising from the GGA and HSE calculations reveal an almost identical decrease of the gap on increasing thickness of the LAO layer. However, the differences

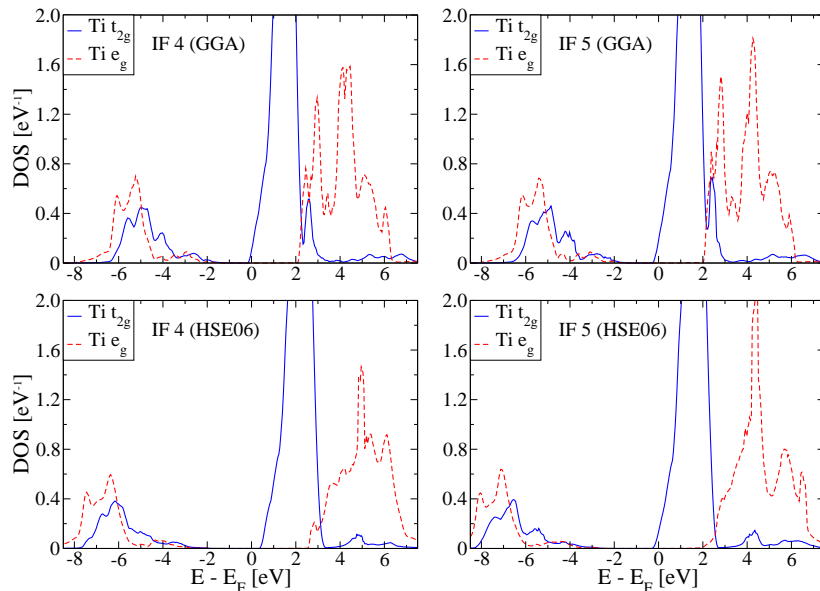


FIG. 3. Projected t_{2g} and e_g DOSs for the Ti1 atom.

between both approaches go beyond a rather simple rigid band shift. According to Fig. 2 the total densities of states show a remarkable qualitative difference especially for the conduction bands. This is explored in more detail in the subsequent analysis of the projected densities of states.

In agreement with the general picture developed in previous work, the bottom of the conduction band (which eventually gets pinned to the Fermi level) traces back to Ti states, see Fig. 3. In particular, we note that the t_{2g} states are next to the conduction band minimum and therefore are the first to be populated. From the GGA we thus obtain quantitative agreement with the findings in Ref.³⁵. The t_{2g} states are responsible for the interface conductivity. On the other hand, the e_g states, which are located several eV away, are further pushed upwards in energy when the Hartree-Fock exchange is turned on. The two-dimensional nature of the electron gas is reflected by the fact that at the interface the hybridization of the Ti states with the O_b (basal O) states is much stronger than with the O_a (apical O) states, for O atoms bound to the same Ti atom.

In Fig. 4 we present the projected DOS obtained for apical (top) and basal (bottom) O atoms, projected on the in-plane ($p_{x,y}$) and out-of-plane (p_z) components of the p orbitals. In a perfect octahedral symmetry we would expect a similar DOS shape for the in-plane O_a and out-of-plane O_b states. Here, we observe at and right above the Fermi energy a contribution from the $p_{x,y}$ states of O_a . In contrast, the p_z states of the O_a atoms nearly vanish. Hence, the p states of the O_a sites right above the Fermi energy are of mainly t_{2g} character as expected. For the O_b atoms, we observe similar contributions from the $p_{x,y}$ and p_z states, which likewise reflect the t_{2g} symmetry. However, their contribution is

much larger than that of the O_a sites thus clearly confirming the distinct two-dimensional nature of the electronic states. This result is the same for GGA and HSE.

The unoccupied O_a $p_{x,y}$ states at the interface give rise to two peaks close to 5 and 6 eV for all metallic systems shown in the upper part of Fig. 4. These peaks are located at lower energy in the HSE DOS in the case of the insulating system with four LAO unit cells. The out-of-plane O_b p_z orbitals are similar to the in-plane O_a $p_{x,y}$ orbitals. For the basal O atoms we obtain a similar behavior, but the peaks come from both the in-plane and out-of-plane p orbitals.

IV. CONCLUSION

In the present work we have employed semilocal and hybrid functionals to compute the equilibrium geometries and electronic ground states of LAO/STO interfaces comprised of a central STO region and LAO surface regions with varying thicknesses. Our results show that calculations using the GGA and HSE functionals predict an insulator-metal transition for thicknesses of three to four unit cells and four to five unit cells of LAO, respectively. While the overall thickness dependence of the electronic structure obtained from both approaches is similar, the main difference results from the increased optical band gap. Importantly, the shapes of the (partial) densities of states show substantial deviations for the GGA and HSE functionals. Since hybrid functional calculations (even for metallic systems) can be expected to describe the shapes with higher accuracy than (semi-)local functionals, this fact lays ground for severe doubts on a large number of previous results obtained by GGA and GGA+ U calculations. It is obvious that band gap

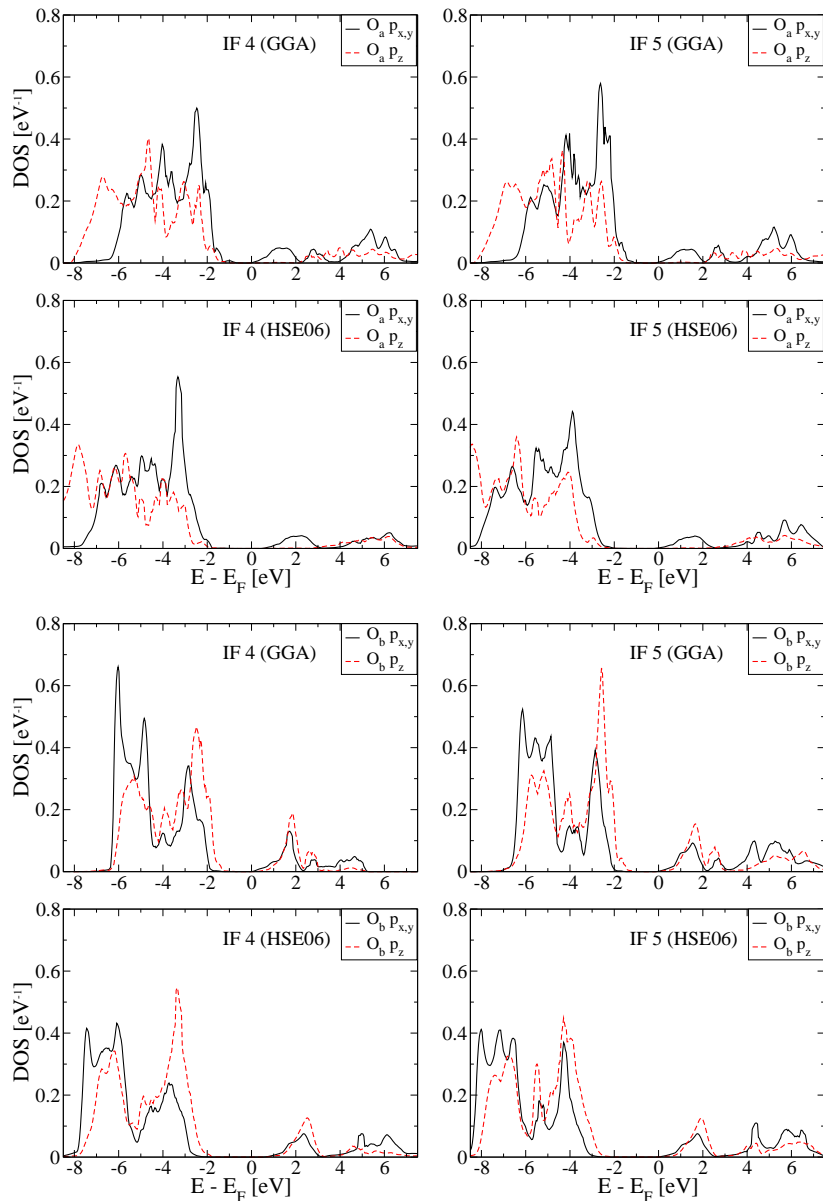


FIG. 4. Projected DOSs for the apical (O_a , between Al and Ti at the interface) and basal (O_b , bonded to Al only) O atoms.

corrections using rigid band shifts cannot be expected to lead to valid results.

ACKNOWLEDGMENTS

We are particularly grateful for vivid discussions with and support from N. Pavlenko, T. Kopp, and J.

Mannhart. The calculations were performed using Material Design's MedeA computational environment. We acknowledge Materials Design Inc. as well as KAUST IT for providing the computational resources for this study. This work was supported by the DFG through TRR 80 and by the BMBF through project No. 03SF0353B.

* Email: udo.schwingenschlogl@kaust.edu.sa

† Present address: Materials Design sarl, 92120 Montrouge, France; Email: veyert@materialsdesign.com

¹ A. Ohtomo and H. Y. Hwang, Nature (London) **427**, 423 (2004).

- ² A. Brinkman, M. Huijben, M. van Zalk, J. Huijben, U. Zeitler, J. C. Maan, W. G. van der Wiel, G. Rijnders, D. H. A. Blank, and H. Hilgenkamp, *Nature Mater.* **6**, 493 (2007).
- ³ A. Ohtomo and H. Y. Hwang, *Nature (London)* **441**, 120 (2006).
- ⁴ A. D. Caviglia, S. Gariglio, C. Cancellieri, B. Sacepe, A. Fete, N. Reyren, M. Gabay, A. F. Morpurgo, and J.-M. Triscone, *Phys. Rev. Lett.* **105**, 236802 (2010).
- ⁵ M. Huijben, G. Rijnders, D. H. A. Blank, S. Bals, S. Van Aert, J. Verbeeck, G. Van Tendeloo, A. Brinkman, and H. Hilgenkamp, *Nature Mater.* **5**, 556 (2006).
- ⁶ N. Nakagawa, H. Y. Hwang, and D. A. Muller, *Nature Mater.* **5**, 204 (2006).
- ⁷ J.-L. Maurice, C. Carretero, M.-J. Casanove, K. Bouzouane, S. Guyard, É. Larquet, and J.-P. Contour, *Phys. Stat. Solidi A* **203**, 2209 (2006).
- ⁸ N. Reyren, S. Thiel, A. D. Caviglia, L. Fitting Kourkoutis, G. Hammerl, C. Richter, C. W. Schneider, T. Kopp, A.-S. Rüetschi, D. Jaccard, M. Gabay, D. A. Muller, J.-M. Triscone, and J. Mannhart, *Science* **317**, 1196 (2007).
- ⁹ P. Delugas, A. Filippetti, V. Fiorentini, D. I. Bilc, D. Fontaine, and P. Ghosez, *Phys. Rev. Lett.* **106**, 166807 (2011).
- ¹⁰ A. Rubano, M. Fiebig, D. Paparo, A. Marino, D. Maccarriello, U. Scotti di Uccio, F. Miletto Granozio, L. Marrucci, C. Richter, S. Paetel, and J. Mannhart, *Phys. Rev. B* **83**, 155405 (2011).
- ¹¹ S. Nazir, M. U. Kahaly, and U. Schwingenschlögl, *Appl. Phys. Lett.* **100**, 201607 (2012).
- ¹² G. Berner, M. Sing, H. Fujiwara, A. Yasui, Y. Saitoh, A. Yamasaki, Y. Nishitani, A. Sekiyama, N. Pavlenko, T. Kopp, C. Richter, J. Mannhart, S. Suga, and R. Claessen, *Phys. Rev. Lett.* **110**, 247601 (2013).
- ¹³ G. Cheng, P. F. Siles, F. Bi, C. Cen, D. F. Bogorin, C. W. Bark, C. M. Folkman, J.-W. Park, C.-B. Eom, G. Medeiros-Ribeiro, and J. Levy, *Nat. Nanotechnol.* **6**, 343 (2011).
- ¹⁴ B. Förg, C. Richter, and J. Mannhart, *Appl. Phys. Lett.* **100**, 053506 (2012).
- ¹⁵ M. Breitschaft, V. Tinkl, N. Pavlenko, S. Paetel, C. Richter, J. R. Kirtley, Y. C. Liao, G. Hammerl, V. Eyert, T. Kopp, and J. Mannhart, *Phys. Rev. B* **81**, 153414 (2010).
- ¹⁶ H. Chen, A. M. Kolpak, and S. Ismail-Beigi, *Adv. Mater.* **22**, 2881 (2010).
- ¹⁷ S. Thiel, G. Hammerl, A. Schmehl, C. W. Schneider, and J. Mannhart, *Science* **313**, 1942 (2006).
- ¹⁸ M. Sing, G. Berner, K. Goß, A. Müller, A. Ruff, A. Wetscherek, S. Thiel, J. Mannhart, S. A. Pauli, C. W. Schneider, P. R. Willmott, M. Gorgoi, F. Schäfers, and R. Claessen, *Phys. Rev. Lett.* **102**, 176805 (2009).
- ¹⁹ A. Kalabukhov, R. Gunnarsson, J. Börjesson, E. Olsson, T. Claeson, and D. Winkler, *Phys. Rev. B* **75**, 121404 (2007).
- ²⁰ N. Pavlenko, T. Kopp, E. Y. Tsymbal, G. A. Sawatzky, and J. Mannhart, *Phys. Rev. B* **85**, 020407 (2012).
- ²¹ N. Pavlenko, T. Kopp, E. Y. Tsymbal, J. Mannhart, and G. A. Sawatzky, *Phys. Rev. B* **86**, 064431 (2012).
- ²² M. Basletic, J.-L. Maurice, C. Carretero, G. Herranz, O. Copie, M. Bibes, E. Jaquet, K. Bouzouane, S. Fusil, and A. Barthelemy, *Nature Mater.* **7**, 621 (2008).
- ²³ R. Pentcheva and W. E. Pickett, *Phys. Rev. B* **78**, 205106 (2008).
- ²⁴ R. Pentcheva and W. E. Pickett, *Phys. Rev. Lett.* **102**, 107602 (2009).
- ²⁵ U. Schwingenschlögl and C. Schuster, *Europhys. Lett.* **81**, 17007 (2008).
- ²⁶ U. Schwingenschlögl and C. Schuster, *Europhys. Lett.* **86**, 27005 (2009).
- ²⁷ N. Pavlenko and T. Kopp, *Surf. Sci.* **605**, 1114 (2011).
- ²⁸ K. Janicka, J. P. Velev, and E. Y. Tsymbal, *Phys. Rev. Lett.* **102**, 106803 (2009).
- ²⁹ G. Kresse and J. Furthmüller, *Phys. Rev. B* **54**, 11169 (1996); *Comput. Mater. Sci.* **6**, 15 (1996).
- ³⁰ J. P. Perdew, K. Burke, and M. Ernzerhof, *Phys. Rev. Lett.* **77**, 3865 (1996).
- ³¹ A. Seidl, A. Görling, P. Vogl, J. A. Majewski, and M. Levy, *Phys. Rev. B* **53**, 3764 (1996).
- ³² J. Heyd, G. E. Scuseria, and M. Ernzerhof, *J. Chem. Phys.* **118**, 8207 (2003), *J. Chem. Phys.* **124**, 219906 (2006).
- ³³ P. E. Blöchl, *Phys. Rev. B* **50**, 17953 (1994).
- ³⁴ G. Kresse and D. Joubert, *Phys. Rev. B* **59**, 1758 (1999).
- ³⁵ R. Pentcheva and W. E. Pickett, *Phys. Rev. B* **74**, 035112 (2006).